Spin-wave mode profiles versus surface/interface conditions in ferromagnetic Fe/Ni layered composites

2003 J. Phys.: Condens. Matter 15 2449

(http://iopscience.iop.org/0953-8984/15/17/303)

INSTITUTE OF PHYSICS PUBLISHING JOURNAL OF PHYSICS: CONDENSED MATTER

J. Phys.: Condens. Matter **15** (2003) 2449–2469 PII: S0953-8984(03)58995-0

Spin-wave mode profiles versus surface/interface conditions in ferromagnetic Fe/Ni layered composites

M Krawczyk[1], H Puszkarski[1], J-C S Lévy[2] and D Mercier[2]

[1] Surface Physics Division, Faculty of Physics, Adam Mickiewicz University, ulica Umultowska 85, Poznań, 61-614 Poland
[2] Laboratoire de Physique Théorique de la Matière Condensée, case 7020, Université Paris 7, 2 place Jussieu, 75251 Paris Cédex 05, France

E-mail: krawczyk@amu.edu.pl

Received 31 January 2003
Published 22 April 2003
Online at stacks.iop.org/JPhysCM/15/2449

Abstract

Spin-wave excitations in ferromagnetic layered composite ($AB\cdots BA$; A and B being different homogeneous ferromagnetic materials) are analysed theoretically, by means of the transfer matrix approach. The properties of multilayer spin-wave mode profiles are discussed in relation to multilayer characteristics, such as the filling fraction and the exchange or magnetization contrast; also, surface spin pinning conditions and dipolar interactions are taken into account. The interface conditions are satisfied by introducing an effective exchange field expressed by interface gradients of the exchange constant and the magnetization. This approach provides an easy way to find frequencies and amplitudes of standing spin waves in the multilayer. The developed theory is applied to interpretation of spin wave resonance (SWR) spectra obtained experimentally by Chambers *et al* in two systems: a bilayer Fe/Ni and a trilayer Ni/Fe/Ni, in perpendicular (to the multilayer surface) configuration of the applied magnetic field. By fitting the SWR spectra obtained experimentally and those found numerically, the surface anisotropies are estimated on multilayer surfaces; then, the observed resonance lines are identified as associated with bulk, surface or interface modes. The theory can be extended to a general case of any multi-component layered system.

1. Introduction

The interest in periodic composite materials, such as photonic [1–4], phononic [5–9] or magnonic [10–13] crystals, has been growing systematically over the last few years. Besides two- and three-dimensional periodic composites, multilayer systems (providing an example of the simplest one-dimensional composite) are studied intensively. In particular, many surveys deal with magnetic multilayers [14–23]. The reason for this special theoretical interest is that in

magnetic layered composites the local magnetic anisotropy, short-range exchange interactions and long-range dipolar forces are competing to determine static and dynamic properties of such materials. As a result, the magnetic arrangement in composite materials is generally complex. In a particular case with a saturating field applied, this arrangement becomes trivial, all spins being parallel, but the dynamic properties remain not obvious. This is the case considered here; we focus on dynamic properties, such as the resonance frequencies and the magnon profiles, which determine the resonance intensities. A complete discrete treatment of a layered system is developed in this paper, in order to obtain in a clear way the magnon profiles within a layered composite.

The example layered systems to be theoretically studied here are provided by Ni/Fe multilayers, whose experimental investigation, using Brillouin scattering [24–26] or ferromagnetic resonance [27–30], is extensively reported in the literature. The spin wave resonance (SWR) spectra resulting from our computations agree with the ferromagnetic resonance measurements performed by Chambers *et al* [31]. Though here limited to systems containing only iron and nickel layers, our method can be applied to any ferromagnetic layered systems.

2. The discretized Landau–Lifshitz equation approach

The applied saturating field makes the direction of the static magnetization, $\vec{M}_l^S$, parallel everywhere (because of the weakness of the magnetic excitation) in the multilayer ABA $\cdots$ A and is perpendicular to the dynamic component $\vec{m}_l$ of the magnetization, which depends on the plane number l, with the following obvious relation for the total magnetization:

$$\vec{M}_l = \vec{M}_l^S + \vec{m}_l. \tag{1}$$

The Landau–Lifshitz (LL) equation reads

$$\frac{\partial \vec{M}_l}{\partial t} = \gamma \mu_0 \vec{M}_l \times \vec{H}_{eff,l}. \tag{2}$$

Taking a resonant solution with $\vec{m}_l \approx \exp(-\mathrm{i}\omega t)$, one obtains

$$-\mathrm{i}\omega \vec{m}_l = \gamma \mu_0 (\vec{M}_l^S + \vec{m}_l) \times \vec{H}_{eff,l} \tag{3}$$

with the local effective field, $\vec{H}_{eff,l}$, having the following form [10–12]:

$$\vec{H}_{eff,l} = \vec{H}_0 + \vec{h}_l + \frac{2}{\mu_0}\left(\vec{\nabla} \cdot \frac{A_l}{M_l^{S\,2}}\vec{\nabla}\right)\vec{m}_l, \tag{4}$$

where $\vec{H}_0$ is the applied magnetic field, $\vec{h}_l$ is the dipolar field, M_l^S is the saturated magnetization and A_l is the local exchange constant. In SWR there is no wave propagation in the layer (since $\vec{k}_\parallel \equiv 0$) and the problem becomes one dimensional; both the dynamic component $\vec{m}_l$ of the magnetization and the dipolar field $\vec{h}_l$ depend only on the plane number l.

In the one-dimensional discrete approach to the layered composite material the local effective field given by equation (4) can be expressed as follows:

$$\vec{H}_{eff,l} = \vec{H}_0 + \vec{h}_l + \frac{2}{\mu_0 a^2}\left[\frac{A_{l+1}}{M_{l+1}^{S\,2}}\vec{m}_{l+1} - \left(\frac{A_{l+1}}{M_{l+1}^{S\,2}} + \frac{A_l}{M_l^{S2}}\right)\vec{m}_l + \frac{A_l}{M_l^{S2}}\vec{m}_{l-1}\right], \tag{5}$$

where a is the lattice parameter in the composite material. It is useful to introduce the effective local parameter

$$J_l = \frac{2A_l}{\mu_0 a^2 M_l^{S2}} \tag{6}$$

to obtain a more compact expression of the effective field:

$$\vec{H}_{eff,l} = \vec{H}_0 + \vec{h}_l + [J_{l+1}\vec{m}_{l+1} - (J_{l+1} + J_l)\vec{m}_l + J_l\vec{m}_{l-1}]. \tag{7}$$

From this formula we obtain the following four expressions for effective fields, respectively, in component A, in component B, and at the interfaces AB and BA:

$$\vec{H}^{A}_{eff,l} = \vec{H}_0 + \vec{h}_l + [J_A\vec{m}_{l+1} - (2J_A)\vec{m}_l + J_A\vec{m}_{l-1}], \tag{8}$$

$$\vec{H}^{B}_{eff,l} = \vec{H}_0 + \vec{h}_l + [J_B\vec{m}_{l+1} - (2J_B)\vec{m}_l + J_B\vec{m}_{l-1}], \tag{9}$$

$$\vec{H}^{AB}_{eff,l} = \vec{H}_0 + \vec{h}_l + [J_B\vec{m}_{l+1} - (J_B + J_A)\vec{m}_l + J_A\vec{m}_{l-1}], \tag{10}$$

$$\vec{H}^{BA}_{eff,l} = \vec{H}_0 + \vec{h}_l + [J_A\vec{m}_{l+1} - (J_A + J_B)\vec{m}_l + J_B\vec{m}_{l-1}]. \tag{11}$$

3. Calculation of thin film dipolar fields

In this section we concentrate on the calculation of the dipolar field $\vec{h}_l$. For this purpose we consider a set of magnetic moments $\mu_{\vec{r}}$ placed regularly in sites $\vec{r}$ of a thin-film crystal lattice of simple cubic structure. Let the crystal surface be the (y, z)-plane of a Cartesian reference system, with the x-axis perpendicular to this plane. The thin film is assumed to be infinite in plane (y, z), but the number of lattice planes perpendicular to the surface is finite. The reference point $(0, 0, 0)$ will be placed in one of the lattice sites; from the analysis presented below it will become clear that the position of this site can be chosen *arbitrarily*.

Magnetic field $\vec{h}_0 \equiv \vec{h}_{(0,0,0)}$ produced by all the dipoles in the reference point is described by a classical formula (obtained using the linear approximation [35]), having the following form in SI units:

$$\vec{h}_0 = \frac{1}{4\pi}\sum_{\vec{r}\neq 0}\frac{3\vec{r}(\vec{\mu}_{\vec{r}}\cdot\vec{r}) - \vec{\mu}_{\vec{r}}r^2}{r^5}; \tag{12}$$

the above sum involves all the sites *except* the reference point ($\vec{r} \equiv 0$). If the lattice planes parallel to the surface are numbered with index n, the position of the sites in which the magnetic moments are located is defined by a set of three integers (n, p, q) satisfying the following relations:

$$\vec{r} = a_c[n, p, q], \qquad r = a_c\sqrt{n^2 + p^2 + q^2}; \tag{13}$$

a_c is the lattice constant, and $\vec{r}_{\parallel} = a_c[p, q]$ is the site vector within a plane. Through inserting the above equations into (12) we obtain

$$\begin{aligned}\vec{h}_0 &= \frac{1}{4\pi}{\sum_{[n,p,q]}}'\left[\frac{3a_c(n\vec{i} + p\vec{j} + q\vec{k})(\vec{\mu}_{\vec{r}}\cdot a_c(n\vec{i} + p\vec{j} + q\vec{k}) - \vec{\mu}_{\vec{r}}a_c^2(n^2 + p^2 + q^2)}{(a_c\sqrt{n^2 + p^2 + q^2})^5}\right] \\ &= \frac{1}{4\pi}{\sum_{[n,p,q]}}'\left[3\frac{\vec{i}(\mu^x_{\vec{r}}n^2 + \mu^y_{\vec{r}}np + \mu^z_{\vec{r}}nq) + \vec{j}(\mu^x_{\vec{r}}np + \mu^y_{\vec{r}}p^2 + \mu^z_{\vec{r}}pq)}{a_c^3(n^2 + p^2 + q^2)^{\frac{5}{2}}}\right. \\ &\quad \left. + \frac{\vec{k}(\mu^x_{\vec{r}}nq + \mu^y_{\vec{r}}pq + \mu^z_{\vec{r}}q^2) - (\mu^x_{\vec{r}}\vec{i} + \mu^y_{\vec{r}}\vec{j} + \mu^z_{\vec{r}}\vec{k})(n^2 + p^2 + q^2)}{a_c^3(n^2 + p^2 + q^2)^{\frac{5}{2}}}\right],\end{aligned} \tag{14}$$

where the sum over $\vec{r}$ is replaced by the triple sum over indices $[n, p, q]$ $\left(\sum_{\vec{r}} \equiv \sum_{[n,p,q]}\right)$; the prime $(')$ at the sum symbol means that the reference point is excluded from the sum. As the site distribution within each plane is symmetric with respect to site $(n, 0, 0)$, each site (p, q) has its negative counterpart $(-p, -q)$. Consequently, in sum (14) all the terms in which p and

q appear in odd powers are compensated, and (14) can be re-written as follows:

$$\begin{aligned}\vec{h}_0 = \frac{1}{4\pi}\sum_{[n,p,q]}{}' \Bigg[& 3\frac{\vec{i}\mu_{\vec{r}}^{x} n^2 + \vec{j}\mu_{\vec{r}}^{y} p^2 + \vec{k}\mu_{\vec{r}}^{z} q^2}{a_c^3 (n^2+p^2+q^2)^{\frac{5}{2}}} \\ & - \frac{\vec{i}\mu_{\vec{r}}^{x}(n^2+p^2+q^2) + \vec{j}\mu_{\vec{r}}^{y}(n^2+p^2+q^2) + \vec{k}\mu_{\vec{r}}^{z}(n^2+p^2+q^2)}{a_c^3 (n^2+p^2+q^2)^{\frac{5}{2}}} \Bigg] \\ = \frac{1}{4\pi}\sum_{[p,q,n]}{}' & \\ \times \Bigg[& \frac{\vec{i}\mu_{\vec{r}}^{x}(2n^2-p^2-q^2) + \vec{j}\mu_{\vec{r}}^{y}(-n^2+2p^2-q^2) + \vec{k}\mu_{\vec{r}}^{z}(-n^2-p^2+2q^2)}{a_c^3 (n^2+p^2+q^2)^{\frac{5}{2}}} \Bigg].\end{aligned} \tag{15}$$

Further simplification will be obtained using double sums over p and q for a given plane n (within the square of a size $2La_c \times 2La_c$):

$$I_n(L) \equiv \sum_{p,q} \frac{n^2}{(n^2+p^2+q^2)^{5/2}} \qquad \text{for } n \neq 0, \tag{16}$$

$$\begin{aligned} J_n(L) &\equiv \sum_{p,q} \frac{p^2}{(n^2+p^2+q^2)^{5/2}} \equiv \sum_{p,q} \frac{q^2}{(n^2+p^2+q^2)^{5/2}} \\ &\equiv \frac{1}{2}\sum_{p,q} \frac{p^2+q^2}{(n^2+p^2+q^2)^{5/2}} \qquad \text{for } n \neq 0, \end{aligned} \tag{17}$$

$$K_n(L) \equiv I_n(L) - J_n(L) \qquad \text{for } n \neq 0; \tag{18}$$

$$\begin{aligned} K_0(L) &\equiv \sum_{p,q}{}' \frac{p^2}{(p^2+q^2)^{5/2}} \equiv \frac{1}{2}\sum_{p,q}{}' \frac{p^2+q^2}{(p^2+q^2)^{5/2}} \\ &\equiv \frac{1}{2}\sum_{p,q}{}' \frac{1}{(p^2+q^2)^{3/2}} \qquad \text{for } n = 0. \end{aligned} \tag{19}$$

The equality of the two sums in (17) is a consequence of the fact that $0x$ is a fourfold symmetry axis for each lattice plane.

We shall now assume that all the magnetic moments within a single plane n are identical, i.e.

$$\vec{\mu}_n \equiv \vec{\mu}_{[n,p,q]}, \qquad \text{for any } p \text{ and } q. \tag{20}$$

Using (16)–(20) we can transform (15) to the following form:

$$\vec{h}_0 = \frac{1}{4\pi}\sum_{n\neq 0} K_n \frac{2\vec{i}\mu_n^x - \vec{j}\mu_n^y - \vec{k}\mu_n^z}{a_c^3} + K_0 \frac{1}{4\pi}\frac{-2\vec{i}\mu_0^x + \vec{j}\mu_0^y + \vec{k}\mu_0^z}{a_c^3}. \tag{21}$$

Note that by assuming $\vec{\mu}_n \equiv \vec{\mu}_{\vec{r}}$ magnetostatic excitations propagating in the *plane* (y, z) were excluded from our analysis.

Formula (21) can be applied to both finite and infinite (in the plane (y, z)) systems. However, our further investigation will focus on the latter case only, and an infinitely large film will be considered with integers p and q running through the infinite set of values, $p, q \in (-\infty, \infty)$. By this assumption, the sums over p and q in (16) and (17) can be replaced by integrals over polar coordinates (r, θ) within the film plane, according to the following *approximate* recipe:

$$I_n[\infty] \approx \int_0^\infty \int_0^{2\pi} \frac{r\,\mathrm{d}r\,\mathrm{d}\theta}{(n^2+r^2)^{5/2}}, \qquad J_n[\infty] \approx \int_0^\infty \int_0^{2\pi} \frac{r^3\cos^2\theta\,\mathrm{d}r\,\mathrm{d}\theta}{(n^2+r^2)^{5/2}}. \tag{22}$$

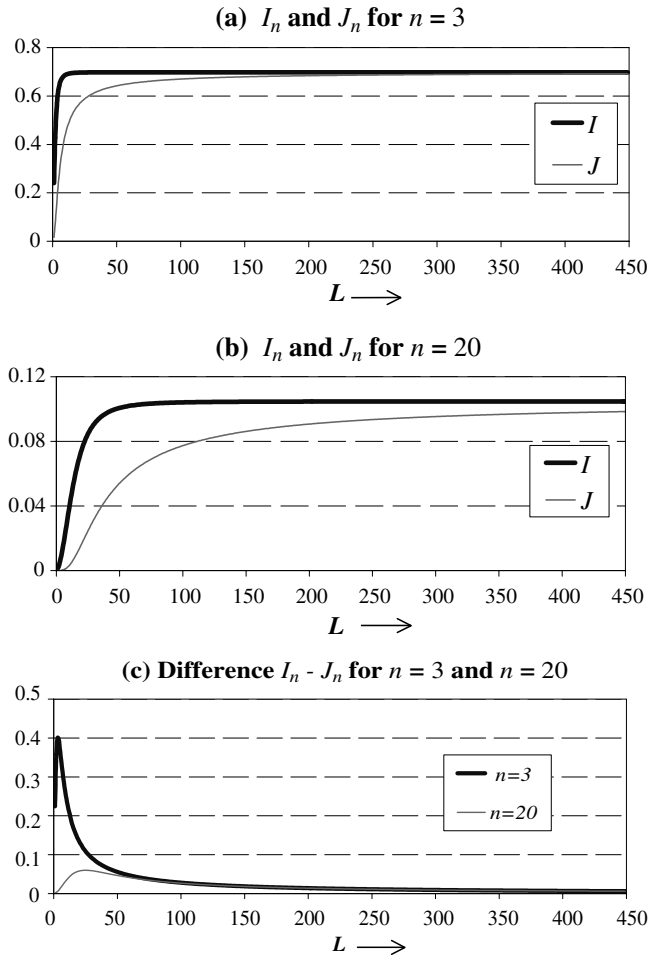

Figure 1. Sums I_n and J_n as well as their difference, $I_n - J_n$, calculated numerically according to definitions (16) and (17) and represented as functions of the structure 'planar' size, determined by L ($-L \leqslant p, q \geqslant L$). The sample size along both $0x$ and $0y$ axes is $2La_c$, a_c being the lattice constant. It is anticipated that for any lattice plane number, n, both sums approach the same limit value when $L \to \infty$.

Both these integrals are immediately found to have the same value, $2\pi/3n$, for any plane number n. Therefore it is legitimate to postulate the following equality:

$$I_n[\infty] = J_n[\infty] = \frac{2\pi}{3n} \qquad (n \neq 0). \tag{23}$$

To verify this conjecture, we calculated *numerically* sums I_n and J_n according to their definitions (16) and (17), for a finite thin film of size $2La_c \times 2La_c$. The resulting values approach *the same* limit when $L \to \infty$, exactly as anticipated in our postulate (23) (see figure 1).

This result is very significant since substitution of (23) in (21) results in complete *vanishing* of the first term representing the contribution to the field $\vec{h}_0$ coming from *all neighbouring* planes. The dipole field calculated within this approximation shall be henceforth denoted by $\vec{h}_0[\infty]$. In its expression according to (21), the value of K_0 (19) corresponds to an *infinite*

plane $n = 0$:

$$\vec{h}_0[\infty] = K_0[\infty]\frac{1}{4\pi}\frac{-2\vec{i}\mu_n^x + \vec{j}\mu_n^y + \vec{k}\mu_n^z}{a_c^3}, \tag{24}$$

where

$$K_0[\infty] \approx \int_{1/2}^{\infty}\int_0^{2\pi}\frac{\cos^2\theta\,\mathrm{d}r\,\mathrm{d}\theta}{r^2} = 2\pi. \tag{25}$$

In the above formula sum K_0 is regarded as approximately equivalent to the respective definite integral; a certain problem appeared at this stage, as the lower limit of integration over the radial variable r was supposed to be chosen so that the reference point, (0, 0, 0), was *excluded* from the integration (as it had been from the corresponding summation). We solved this problem by assuming such a lower limit of integration that the static demagnetization coefficient calculated with the help of (25) corresponded exactly to the classical text-book result of magnetic thin film theory [36].

Since the considered 'zero' plane was chosen arbitrarily, (24) can be regarded as a general formula describing the dipole field in *any* site of an infinitely extended plane l:

$$\vec{h}_l \equiv \vec{h}_0[\infty] = \frac{1}{2}\frac{-2\vec{i}\mu_l^x + \vec{j}\mu_l^y + \vec{k}\mu_l^z}{a_c^3}. \tag{26}$$

It is convenient to introduce in this formula the notion of *magnetization*, a phenomenological quantity, which in the considered case of a simple cubic lattice can be defined as follows:

$$\vec{M}_l = \vec{\mu}_l/a_c^3. \tag{27}$$

Then, (26) can be written in the tensor notation:

$$\vec{h}_l = \tfrac{1}{2}(-2M_l^x\vec{i} + M_l^y\vec{j} + M_l^z\vec{k}) = \frac{1}{2}\begin{pmatrix}-2 & 0 & 0\\ 0 & 1 & 0\\ 0 & 0 & 1\end{pmatrix}\begin{pmatrix}M_l^x\vec{i}\\ M_l^y\vec{j}\\ M_l^z\vec{k}\end{pmatrix}. \tag{28}$$

Let us now consider two particular cases.

Case 1. The applied static field is perpendicular to the film surface

When a static magnetic field is applied perpendicularly to the film surface, the allowed magnetostatic excitations propagate only in the direction of the field. In the coordinate system assumed above (with axis $0x$ oriented along the surface normal and axes $0y$ and $0z$ lying in the surface plane), component M_l^x corresponds to the static magnetization, M_l^S. Thus, (28) takes the following form:

$$\vec{h}_l = \tfrac{1}{2}\begin{pmatrix}-2 & 0 & 0\\ 0 & 1 & 0\\ 0 & 0 & 1\end{pmatrix}\begin{pmatrix}M_l^S\vec{i}\\ m_l^y\vec{j}\\ m_l^z\vec{k}\end{pmatrix}, \tag{29}$$

where m_l^y and m_l^z are dynamical components of the transversal magnetization $\vec{m}_\parallel = m_l^y\vec{j} + m_l^z\vec{k}$.

Case 2: The applied static field lies in the film plane

In this configuration, referred to as *parallel*, the magnetostatic excitations propagate in the direction perpendicular to the applied field. Assuming that axis $0x$ is still perpendicular to the

film plane and axis $0z$ follows the direction of the spontaneous magnetization ($M_l^z \equiv M_l^S$), (28) becomes

$$\vec{h}_l = \frac{1}{2}\begin{pmatrix} -2 & 0 & 0 \\ 0 & 1 & 0 \\ 0 & 0 & 1 \end{pmatrix}\begin{pmatrix} m_l^x \vec{i} \\ m_l^y \vec{j} \\ M_l^S \vec{k} \end{pmatrix}. \tag{30}$$

The above formulae clearly indicate that the magnetic moment precession is circular in the first case, and elliptic in the second one, which is in perfect conformity with the classical result obtained through a macroscopic approach [36].

Below we will focus on the *perpendicular configuration only*, therefore $\vec{h}_l$ will be expressed by the formula (29).

4. The transfer matrix approach

Using the expression (7) in LL equation (3), and expressing $\vec{h}_l$ by magnetizations according to (29), leads to the following equation:

$$-\mathrm{i}\omega\vec{m}_l = \gamma\mu_0(\vec{M}_l^S + \vec{m}_l)\big(\vec{H}_0 - \vec{M}_l^S + \tfrac{1}{2}\vec{m}_l + [J_{l+1}\vec{m}_{l+1} - (J_{l+1} + J_l)\vec{m}_l + J_l\vec{m}_{l-1}]\big). \tag{31}$$

In the linear approximation (assuming $m \ll M^S$, $h \ll H_0$), the terms including $\vec{m}$ squared are neglected, leading to the following *vector* equation:

$$-\mathrm{i}\omega\vec{m}_l = \gamma\mu_0\vec{M}_l^S \times \big[J_{l+1}\vec{m}_{l+1} - (J_{l+1} + J_l)\vec{m}_l + \tfrac{1}{2}\vec{m}_l + J_l\vec{m}_{l-1}\big] + \gamma\mu_0\vec{m}_l \times \big[\vec{H}_0 - \vec{M}_l^S\big] \tag{32}$$

or its equivalent *two scalar equations*:

$$\begin{aligned}\omega m_{l,y} &= \mathrm{i}\gamma\mu_0 M_l^S\big[-J_{l+1}m_{l+1,z} + (J_{l+1} + J_l)m_{l,z} - \tfrac{1}{2}m_{l,z} - J_l m_{l-1,z}\big] \\ &\quad + \mathrm{i}\gamma\mu_0 m_{l,z}(H_0 - M_l^S), \qquad (33)\\ -\mathrm{i}\omega m_{l,z} &= \gamma\mu_0 M_l^S\big[J_{l+1}m_{l+1,y} - (J_{l+1} + J_l)m_{l,y} + \tfrac{1}{2}m_{l,y} + J_l m_{l-1,y}\big] \\ &\quad - \gamma\mu_0 m_{l,y}(H_0 - M_l^S). \qquad (34)\end{aligned}$$

Now, complex quantities $m_l^{\pm}$ are introduced, according to the standard method:

$$\begin{aligned} m_l^+ &= m_{l,y} + \mathrm{i}m_{l,z}, \\ m_l^- &= m_{l,y} - \mathrm{i}m_{l,z}. \end{aligned}$$

Adding and subtracting equations (33) and (34) results in two independent equations for m^+ and m^-, corresponding to spin waves polarized circularly in opposite directions. In further reasoning, we will use the equation with m^+ only:

$$C_l J_{l+1} m_{l+1}^+ + \big[\Omega - C_l(J_{l+1} + J_l) + \tfrac{3}{2}C_l - 1\big]m_l^+ + C_l J_l m_{l-1}^+ = 0, \tag{35}$$

introducing reduced frequency Ω,

$$\Omega = \frac{\omega}{\gamma\mu_0 H_0}, \tag{36}$$

and magnetic stiffness constant,

$$C_l = \frac{M_{S,l}}{H_0}. \tag{37}$$

Equation (35) can be read in a regressive way, in order to define a transfer matrix:

$$m_{l-1}^+ = \frac{[1 + C_l(J_l + J_{l+1} - \frac{3}{2}) - \Omega]}{C_l J_l}m_l^+ - \frac{J_{l+1}}{J_l}m_{l+1}^+ \tag{38}$$

and

$$\begin{pmatrix} m_{l-1}^{+} \\ m_{l}^{+} \end{pmatrix} = \begin{pmatrix} \frac{[1+C_l(J_l+J_{l+1}-\frac{3}{2})-\Omega]}{C_l J_l} & -\frac{J_{l+1}}{J_l} \\ 1 & 0 \end{pmatrix} \cdot \begin{pmatrix} m_{l}^{+} \\ m_{l+1}^{+} \end{pmatrix}. \tag{39}$$

For a composite sample made of two materials A and B, with different exchange constant and magnetic stiffness values, four transfer matrices must be defined: $\hat{t}_A, \hat{t}_B, \hat{t}_{AB}$ and $\hat{t}_{BA}$, according to four effective fields (8)–(11). They are

$$\begin{aligned} \hat{t}_A &= \begin{pmatrix} 2+\frac{1-\Omega-\frac{3}{2}C_A}{C_A J_A} & -1 \\ 1 & 0 \end{pmatrix}, \qquad \hat{t}_B = \begin{pmatrix} 2+\frac{1-\Omega-\frac{3}{2}C_B}{C_B J_B} & -1 \\ 1 & 0 \end{pmatrix}, \\ \hat{t}_{AB} &= \begin{pmatrix} 1+\frac{1-\Omega+C_B(J_A-\frac{3}{2})}{C_B J_B} & -\frac{J_A}{J_B} \\ 1 & 0 \end{pmatrix}, \qquad \hat{t}_{BA} = \begin{pmatrix} 1+\frac{1-\Omega+C_A(J_B-\frac{3}{2})}{C_A J_A} & -\frac{J_B}{J_A} \\ 1 & 0 \end{pmatrix}. \end{aligned} \tag{40}$$

For composite structure ABABABA, where each block A is made up of L_A planes and each block B is made up of L_B planes (see figure 2), the global transfer matrix $\hat{T}$ is defined as follows:

$$\hat{T} = \hat{t}_A^{L_A-1} \cdot \hat{t}_{BA} \cdot \hat{t}_B^{L_B-1} \cdot \hat{t}_{AB} \cdot \hat{t}_A^{L_A-1} \cdots \hat{t}_{BA} \cdot \hat{t}_B^{L_B-1} \cdot \hat{t}_{AB} \cdot \hat{t}_A^{L_A}. \tag{41}$$

The boundary conditions are defined by the pinning equations involving surface pinning parameters a_p and a'_p, related to the well known surface parameters A_{surf} [37–40] (see the appendix for details):

$$m_{-1}^{+} = a_p m_0^{+}, \tag{42}$$

$$m_{L}^{+} = a'_p m_{L-1}^{+}, \tag{43}$$

where (in the case considered here) the total number L is $L = 4L_A + 3L_B$. Thus, the characteristic equation reads

$$(1, -a_p) \cdot \hat{T} \cdot \begin{pmatrix} 1 \\ a'_p \end{pmatrix} = 0. \tag{44}$$

Then, the spin wave mode profiles can be calculated according to the partial transfer matrix, which is deduced from equation (41).

5. The effect of dipolar interactions on the spin wave spectrum

The effect of long-range dipolar interactions on magnetic multilayer spin wave modes is to be examined first. However, in our study, this effect is assumed not to be related to the existence of surface magnetostatic excitations [41–48]. We simply compare the magnon spectra calculated according to (44), where both dipolar (static and dynamic) and exchange fields are considered, with those obtained from equations in which the dynamic dipolar field is neglected and one only takes into account exchange and demagnetization fields. Special attention is paid to the shape of spin wave mode profiles. Conditions for the effect of dipolar field to be negligible will be deduced from this comparison.

In the considered symmetrical multilayer $[\mathrm{Fe/Ni}]_3\mathrm{Fe}$, with the 'lattice' constant $(L_{\mathrm{Fe}} + L_{\mathrm{Ni}})a = 100$ Å and surface spins strongly pinned, the dynamic dipolar interactions are found to cause only minor shifts of exchange spin wave energy branches towards lower frequency values (see figure 3). For non-zero values of magnetization contrast (figure 3), this shift depends on the filling fraction f, defined as the thickness ratio of layer Fe to bilayer Fe/Ni (regarded as the unit cell):

$$f = \frac{L_{\mathrm{Fe}}}{L_{\mathrm{Fe}} + L_{\mathrm{Ni}}}. \tag{45}$$

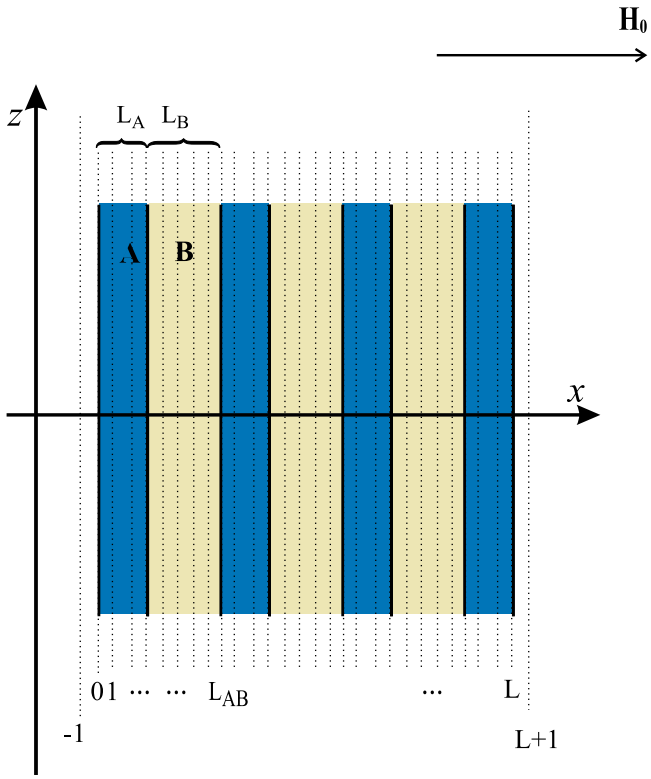

Figure 2. The model of a multilayer composed of $N_A = 4$ sublayers of material A and $N_B = 3$ sublayers of material B. Each sublayer A or B contains L_A or L_B planes respectively. L is the total number of planes in the multilayer. Fictitious planes $l = -1$ and $l = L + 1$ lie beyond the multilayer.

(This figure is in colour only in the electronic version)

For a composite with component materials differing in their exchange constant values only, the shift is insensitive to the filling fraction.

We also notice an effect of the dipolar field on the lowest magnon mode profiles. Figure 4 shows profiles of the first three exchange-dipolar modes (full curve) and the corresponding exchange-demagnetization modes (broken curve), in a system composed of four Fe layers and three Ni layers. As the effect of dipolar field is found to become negligible for higher frequencies (higher modes), we will confine our interest to the lowest mode.

Figure 5 shows profiles of the first spin mode for three values of the filling fraction: $f = 0.1$ (nickel predominating in the multilayer), $f = 0.5$ (all sublayers being of the same thickness) and $f = 0.9$ (Fe predominating). The interface pinning seems to be due to the relatively high magnetization value in iron layers with respect to that in Ni layers ($M_{S_{\mathrm{Fe}}}/M_{S_{\mathrm{Ni}}} \approx 3.0$). Furthermore, we notice that profile deformations are more significant in the inner iron layers than in those close to the surface. In our opinion, this is due to the larger distance between the inner layers and the multilayer external surfaces, where the spins are assumed to be completely pinned.

Furthermore, the effect of dynamic dipole interactions is found to increase with surface spin freedom, especially in layers close to the multilayer surfaces. Figure 6 shows the profile of the lowest spin wave mode in multilayer $[\mathrm{Fe/Ni}]_3\mathrm{Fe}$ with unpinned surface spins; it is worth

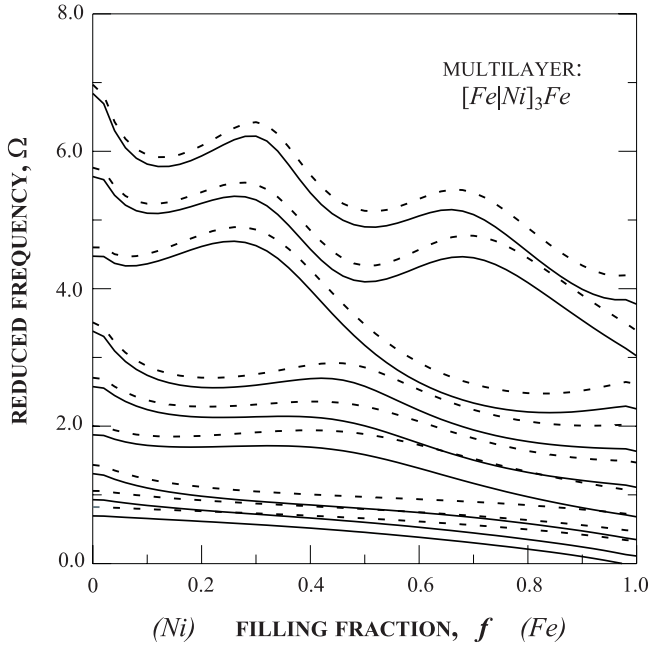

Figure 3. Spin wave mode energy spectrum *versus* filling fraction $f = L_{\mathrm{Fe}}(L_{\mathrm{Fe}}+L_{\mathrm{Ni}})^{-1}$, computed for two cases: with dynamic dipolar field included (full curves) or neglected (broken curves). The considered multilayer Fe/Ni/Fe/Ni/Fe/Ni/Fe represents the case with strong magnetization contrast and strong surface spin pinning, $M_{S_{\mathrm{Fe}}} = 1.752 \times 10^6$ A m^{-1}, $A_{\mathrm{Fe}} = 2.1 \times 10^{-11}$ J m^{-1} and $M_{S_{\mathrm{Ni}}} = 0.61 \times 10^6$ A m^{-1}, $A_{\mathrm{Ni}} = 0.7 \times 10^{-11}$ J m^{-1}.

noticing that for $A_{surf} \geqslant 1.0$ the lowest symmetrical mode corresponds to a surface excitation with maximum amplitude on the multilayer external surfaces. The dipole interactions intensify the spin wave amplitude on the surface, which involves an increase of surface energy and therefore of surface spin freedom too. As a result, the calculated spin wave surface amplitude is higher if dipole interactions are taken into account (full curve), and lower if those interactions are neglected (broken curve). One notes that this discrepancy grows with the surface parameter value.

The effects discussed above have their impact on the SWR spectrum. The SWR intensity is given by the following formula [37]:

$$P(n) = \sum_l |m_l^+(n)|^2, \tag{46}$$

where $m_l^+(n)$ is the normalized nth spin-wave mode amplitude in the lth plane. Figure 7 shows that including the dynamic dipole field in the consideration has a double SWR effect: (a) the whole spectrum is shifted towards lower frequencies, and (b) the relative intensities of the first resonance lines are essentially modified. Hence, including the dipole interactions seems to be necessary especially in calculations for magnetic multilayers with *positive value* of surface anisotropy, i.e. the value evoking surface spin wave modes.

Further on we will focus on low energy states, in which the effect of dipolar field is appreciable. Thus, the interactions to be considered in the following calculations include exchange and demagnetization as well as dynamic dipolar fields. For the excitations studied below we always assume $\mu_0 H_0 = 0.1$ T.

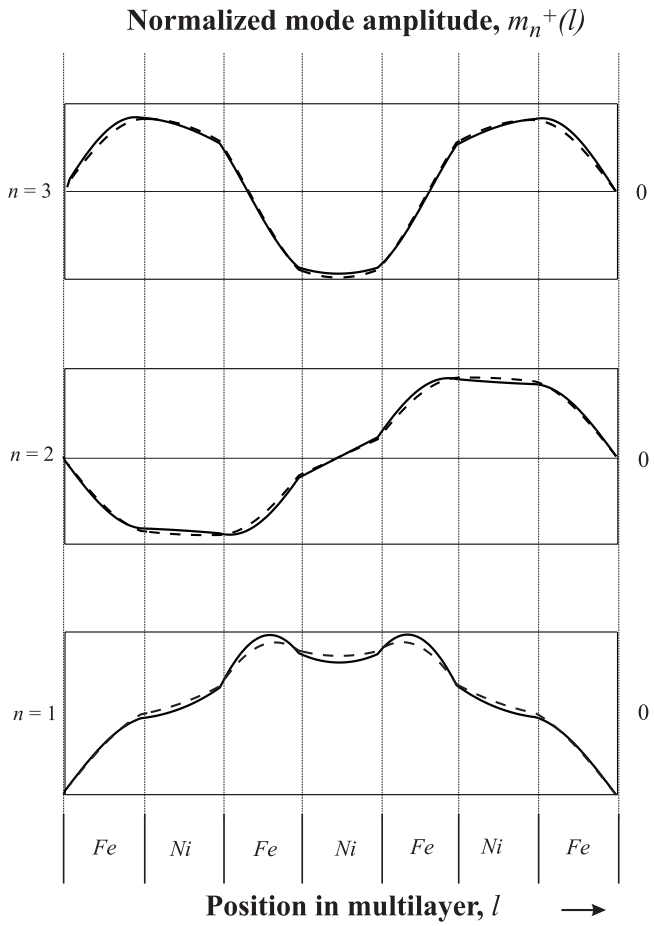

Figure 4. The normalized mode amplitude profiles of exchange-dipolar spin wave modes $n = 1, 2$ and 3 in a $[Fe/Ni]_3Fe$ multilayer (full curves). For comparison, profiles of pure exchange-demagnetization modes are also shown (broken curves). Surface spins are assumed to be strongly pinned, and the filling fraction value is taken as $f = 0.5$.

6. Spin wave mode profiles

Excitations in a multilayer generally behave like those in a homogeneous film. An example is shown in figure 4: in a symmetrical multilayer with surface spins pinned, the modes represent alternately symmetrical and antisymmetrical standing waves with nodes on the surfaces, exactly as in a homogeneous film. The difference is that inside the sample the multilayer profiles do not vary homogeneously, due to perturbations caused by interfaces. Now we are going to study the effect of interfaces (as well as that of surface conditions) on the shape of mode profiles in a multilayer.

Figure 5 shows variations of the first mode profile for different filling fraction values. For all three filling fraction values ($f = 0.1$, 0.5 and 0.9), the profiles preserve their general form of the first harmonic. It should be noticed that all the sublayers show asymmetry in their partial profiles, their amplitudes being the lowest on the side of the closest outer surface. This effect is stronger in iron layers, due to their high magnetization value, but also occurs (although it is

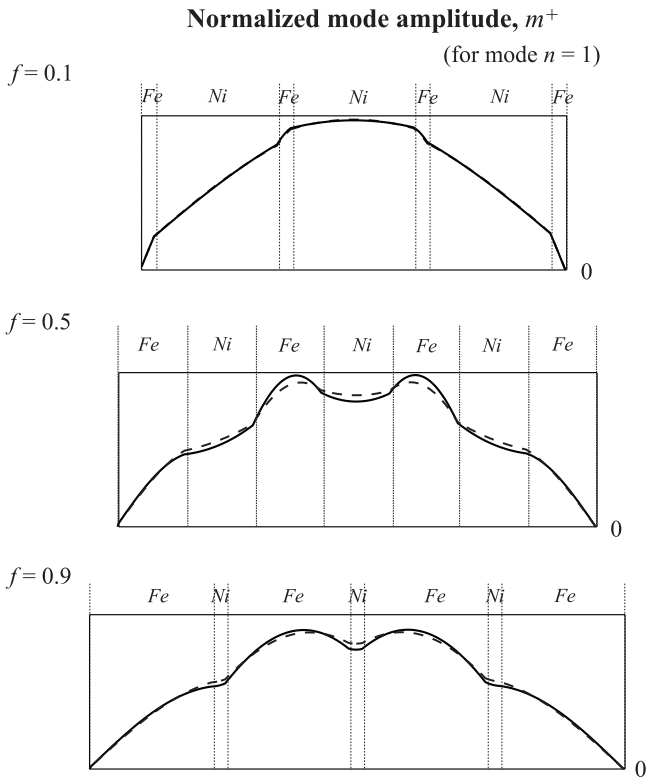

Figure 5. The first mode amplitude profile across the multilayer $[Fe/Ni]_3Fe$ for different values of the filling fraction: $f = 0.1$, 0.5 and 0.9. Profiles obtained for dipolar, demagnetization and exchange fields included (full curves) are juxtaposed with those obtained considering demagnetization and exchange fields only (broken curves). In both cases surface spins are strongly pinned.

much weaker) in Ni layers (cf cases $f = 0.1$ and 0.9 in figure 5); the asymmetry disappears in the central zone. The same is observed in all the higher modes, though the effect decreases as frequency increases.

Figure 8 shows profiles of modes $n = 1$, 4 and 7 (8) in the investigated composite, for two filling fraction values: (a) $f = 0.1$, in which case nickel is the predominating material, and (b) $f = 0.9$, with iron predominating. The lowest ($n = 1$) mode profile (the same as in figure 5) is composed of more or less linear segments, each corresponding to a single sublayer. For $n = 4$ the mode profile segments in the predominant material become sinusoidal arches, the interface amplitude being maximum in Ni (if $f = 0.1$) and minimum (close to zero) in Fe sublayers (if $f = 0.9$). The lowest mode of the third band, $n = 7$, shows similar features. This indicates a strong pinning of the interface spins in Fe layers (i.e. those in contact with nickel), while the Ni interface spins (in contact with iron) show no pinning at all.

7. SWR spectra in iron/nickel bilayers and nickel/iron/nickel trilayers

The above-presented method of calculating spin wave profiles and resonance spectra can be used in interpretation of SWR spectra observed experimentally in ferromagnetic multilayer systems. Through fitting the calculated resonance line intensities and positions

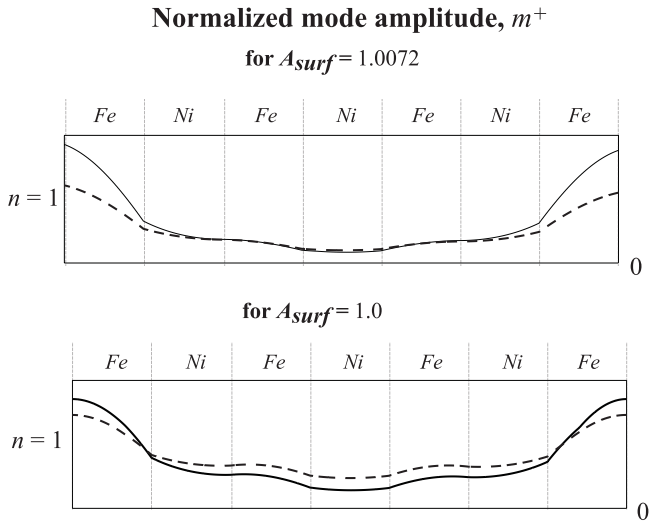

Figure 6. The lowest mode profiles for two surface parameter values, $A_{surf} = 1.0$ and 1.0072, in multilayer $[Fe/Ni]_3Fe$, computed considering dipolar and exchange interactions (full curves), juxtaposed with those obtained considering the exchange field only (broken curves).

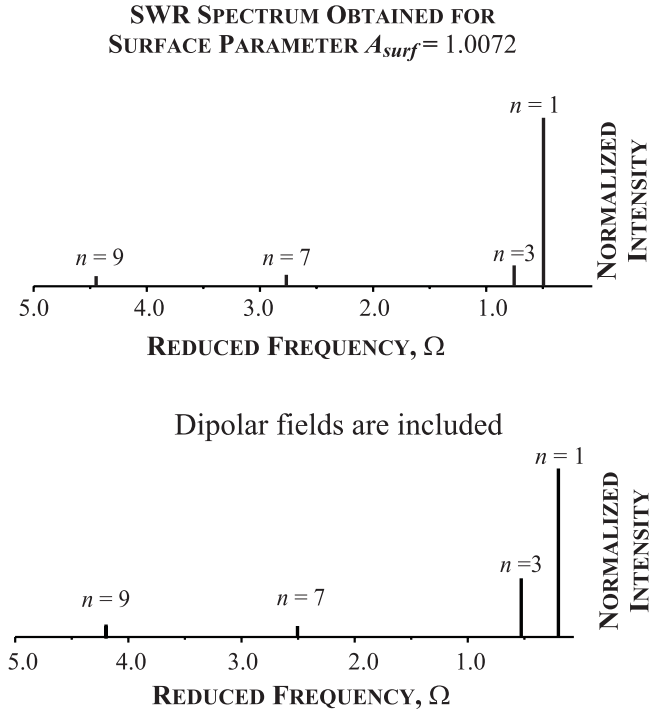

Figure 7. SWR spectrum in the multilayer $[Fe/Ni]_3Fe$ computed considering dipolar and exchange interactions (bottom spectrum), juxtaposed with that obtained considering exchange field only (upper spectrum)—for the case of unpinned surface spins ($A_{surf} = 1.0072$).

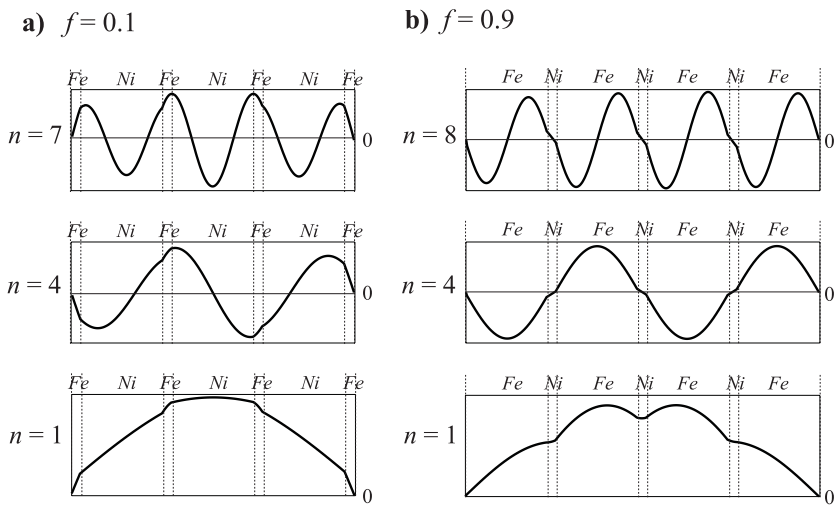

Figure 8. Spin wave mode profiles in [Fe/Ni]$_3$Fe multilayer. (a) Profiles of modes $n = 1, 4$ and 7 obtained for filling fraction value $f = 0.1$ (Ni and Fe sublayer thickness being 90 and 10 Å, respectively). (b) Profiles of modes $n = 1, 4$ and 8 obtained for filling fraction value $f = 0.9$. In both cases surface spins are strongly pinned.

to corresponding experimental results one is able to find surface material parameter values of interest. Below we develop a qualitative analysis of the resonance spectra obtained by Chambers *et al* [31] in bilayer and trilayer systems composed of iron and nickel, estimating the involved surface anisotropy energy. As these experimentally studied systems are asymmetric, in their theoretical treatment it is necessary to introduce two surface parameters, A_s and A_f, corresponding to the substrate interface and the multilayer free surface, respectively.

Figure 9 shows the SWR spectrum calculated for a bilayer Fe/Ni (the respective sublayer thickness values being 100 Å/1500 Å) with the following surface parameter values: substrate interface (LiF/Fe) parameter $A_s = 1.011\,48$, and free surface (Ni/air) parameter $A_f = 1.005\,28$. This spectrum corresponds to that observed experimentally for LiF/Fe/Ni/air and reported in [31]. In our interpretation of this spectrum, mode $n = 1$ lies *beyond* the considered frequency range and its intensity is close to zero (due to its strong surface localization); the most intensive excitation corresponds to mode $n = 2$, which is of bulk character within the iron sublayer and becomes localized (near the external surface) in the nickel sublayer.

We propose an analogical interpretation of the SWR spectrum in LiF/Ni/Fe/air (see figure 10). Our theoretical spectrum, obtained through fitting the surface parameter values, corresponds to that observed experimentally [31]. The results of this fitting indicate rather a high degree of surface spin freedom: the surface parameter value in Ni (on its interface with the LiF substrate) is $A_s = 1.024\,64$, while the free surface parameter value in Fe is found to be $A_f = 1.045\,92$. As in the preceding case, mode $n = 1$ is invisible here. Mode $n = 2$, the first to be noticeable in the resonance spectrum, is localized in Ni at the substrate interface, whereas mode $n = 3$ is also localized in the same layer, but at the other interface, Ni/Fe.

As nickel is the predominating material in the studied bilayers (nickel to iron layer thickness ratio is 15 to 1), it is from the Ni layer excitations that the principal contribution to the resonance line intensity originates. Therefore, a *single* Ni layer with *effective* surface parameters on interfaces (LiF/Fe)/Ni and Ni/(Fe/air) can be considered instead of the actual bilayer (this approach was used for example in [49] to study ferromagnetic resonance in

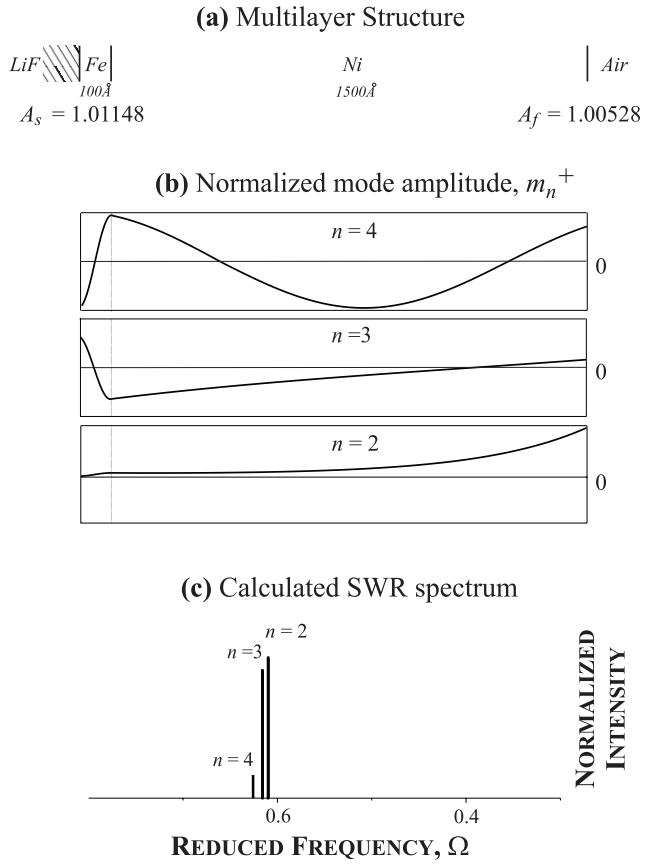

Figure 9. SWR spectrum and profiles of the first three noticeable modes computed for the system LiF/Fe/Ni/air, depicted above. The respective surface parameter values, $A_s = 1.011\,48$, $A_f = 1.005\,28$, are found through fitting this spectrum to that obtained experimentally by Chambers *et al* [31].

a system consisting of a *thick* iron layer covered with a *thin* nickel film). The following effective pinning parameter values were found for the bilayers considered in this study: for the interface Ni/(Fe/air) the increase of surface parameter value A_f from 1.005 28 to 1.014 08 seems to indicate that the iron interlayer inserted between nickel and air increases nickel surface anisotropy, nearly doubling its value, while inserting the same interlayer between nickel and lithium fluoride (the interface (Li/Fe)/Ni) substantially reduces surface anisotropy since the surface parameter A_s decreases from 1.024 64 to 1.002 82.

The above-mentioned values of surface parameters in Ni were used in calculating the resonance spectra in LiF/Ni/Fe/Ni/air trilayers with the respective magnetic sublayer thickness values 250 Å/100 Å/1250 Å (see figure 11) and 1250 Å/100 Å/250 Å (see figure 12). Our spectra fit with those obtained experimentally [31], involving only slight modifications of the surface parameter values found from the bilayer spectrum. This confirms the correctness of our calculation procedure; moreover, through the profiles found, each resonance line can be univocally interpreted in the trilayer spectrum: all the first three lines are *surface* modes confined in nickel sublayers, localized, respectively, on the Ni/Fe interface, substrate interface and free surface.

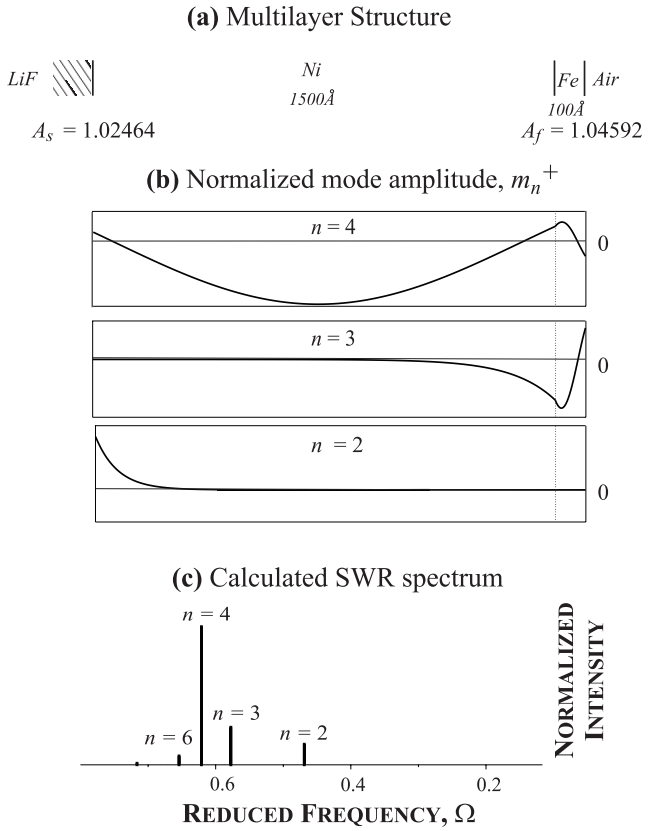

Figure 10. SWR spectrum and profiles of the first three noticeable modes computed for the system LiF/Ni/Fe/air, depicted above. The respective surface parameter values, $A_s = 1.024\,64$, $A_f = 1.045\,92$, are found through fitting this spectrum to that obtained experimentally by Chambers *et al* [31].

8. Conclusions

The calculation procedure developed in this study is based on the transfer matrix approach and allows us to compute SWR spectra in ferromagnetic multilayers, taking dipole interactions into account. The dynamic component of the dipole field, expressed as a function of magnetization, is related to its transversal component through the magnetic susceptibility tensor. As shown above, this tensor has a particularly simple form for the magnetization vector being either perpendicular or parallel to the multilayer surface. Only the perpendicular configuration was considered in detail, and resonance computations were performed for multilayer systems consisting of Fe and Ni sublayers.

The dipole interactions are found to produce a homogeneous shift of the spin wave excitation energy branches, the effect strongly depending on the filling fraction and the magnetization contrast between constituent materials. Moreover, the spin wave profile deformation due to the dipole field is found to be the most significant in the low frequency range, and to depend on surface conditions: the higher the degree of surface spin freedom, the more significantly modified are the low energy mode profiles. Obviously, these dipole-related deformations of spin wave amplitude distribution involve modifications of resonance line

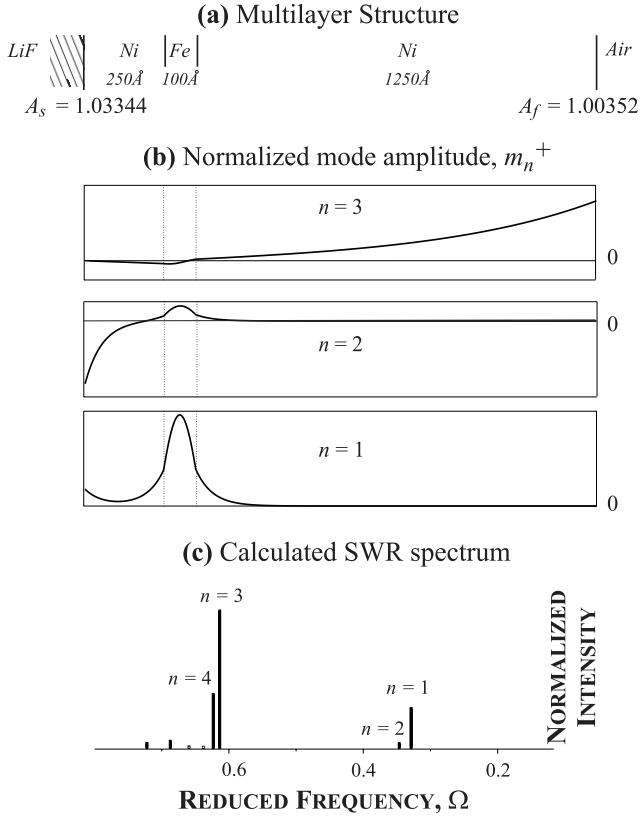

Figure 11. The theoretically found SWR spectrum and profiles of the first three modes in the trilayer LiF/Ni/Fe/Ni/air (depicted above); the respective magnetic sublayer thickness values are 250 Å/100 Å/1250 Å. This theoretical spectrum was fitted to that obtained experimentally by Chambers *et al* [31], resulting in surface parameter values $A_s = 1.033\,44$ and $A_f = 1.003\,52$.

intensity as well. For all these reasons, we decided to include the effect of dipole interactions in our calculations of SWR spectra, which were subsequently compared to the corresponding experimental results [31].

A two-step procedure was followed in order to compare our theoretical SWR spectra with those obtained experimentally: first, surface parameter estimate values were deduced from resonance spectra in LiF/Fe/Ni/air and LiF/Ni/Fe/air *bilayers*; next, the values obtained were used to calculate *trilayer* SWR spectra. These spectra showed a very good qualitative fit with those obtained experimentally, which indicates that our estimates of surface anisotropy energy values are reliable. The estimated values of surface anisotropy constant K_S, found using our theory for different Fe and Ni interfaces, are detailed in table 1. These values correspond with the results reported by other authors (see [50, 51]).

An interesting feature of interface spin pinning was revealed in this study. This pinning is due to the magnetization and exchange contrasts on the interface, and possible to deduce, at least qualitatively, from the shape of spin wave profiles. The profiles obtained within this study indicate that Fe spins in contact with Ni become strongly pinned, while Ni spins in contact with Fe seem to recover freedom.

In our next study we are going to extend the research presented above to any configuration of the magnetic field with respect to the multilayer surface.

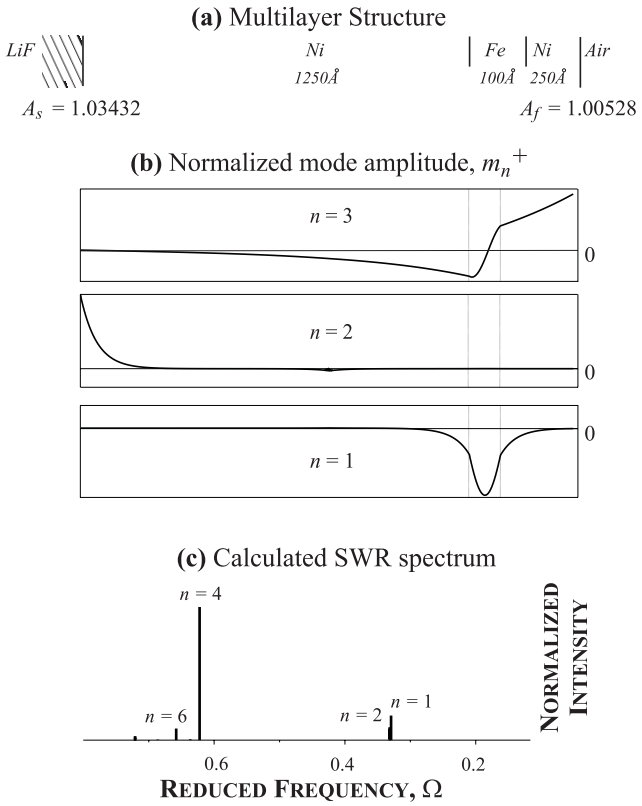

Figure 12. The theoretically found SWR spectrum and profiles of the first three modes in the trilayer LiF/Ni/Fe/Ni/air (depicted above); the respective magnetic sublayer thickness values are 1250 Å/100 Å/250 Å. This theoretical spectrum was fitted to that obtained experimentally by Chambers *et al* [31], resulting in surface parameter values $A_s = 1.034\,32$ and $A_f = 1.005\,82$.

Table 1. Surface anisotropy K_S(erg cm^{-2}) values for different iron and nickel interfaces deduced from theoretical interpretation of SWR spectra reported in [31].

Interface	$K_S(10^{-3}$ J m$^{-2})$
Ni/air	<0.1
LiF/Ni	0.7–0.95
Fe/air	>3.0
LiF/Fe	0.85
Ni/(Fe/air)	0.35
Effective value	
(LiF/Fe)/Ni	<0.10
Effective value	

Acknowledgment

This study was supported by the Polish Committee for Scientific Research, grant No 2 PO3B 120 23.

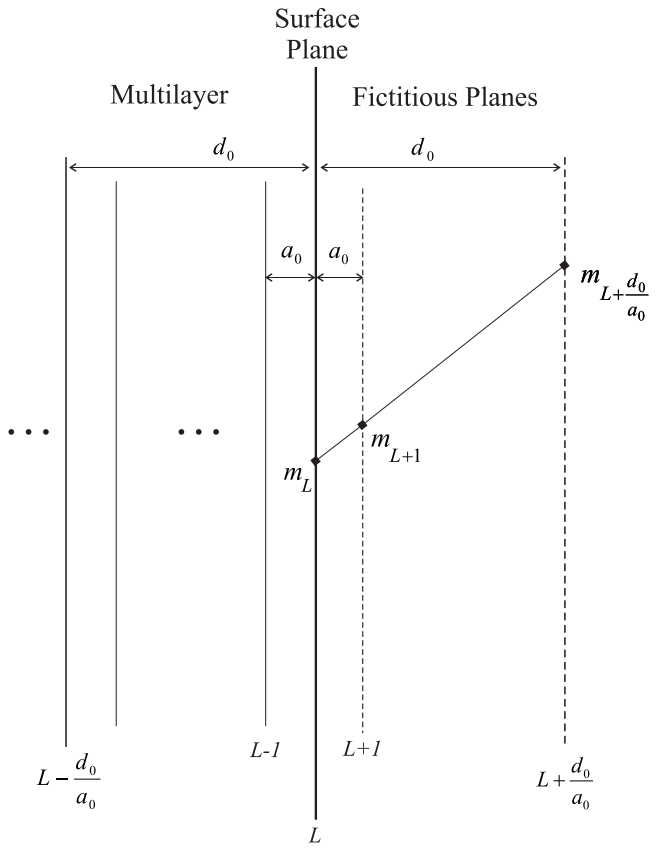

Figure A.1. Schematically depicted interpolation supplying the base for deriving the relation between the actual surface parameter A_{surf} and parameter a_p used in our numerical calculations.

Appendix. Derivation of the surface parameter formula

There is a simple relation between surface parameter A_{surf} and surface anisotropy constant K_S[37]:

$$A_{surf} = 1 + \frac{K_S d_0}{A}, \tag{A.1}$$

d_0 being the distance between neighbouring atomic planes in the direction perpendicular to the surface, and A being the exchange constant. In this definition, the surface parameter is the ratio of the dynamic magnetization value on a multilayer external surface to that of a fictitious atomic plane (see figure A.1):

$$m_{L+\frac{d_0}{a_0}} = A_{surf} m_L. \tag{A.2}$$

However, in the numerical computations performed in this study, another surface parameter is used, a_p, defined as the ratio of magnetization values of a multilayer surface and an arbitrary *fictitious plane* $(L + 1)$:

$$m_{L+1} = a_p m_L, \tag{A.3}$$

the distance a_0 between this fictitious plane and the surface being *arbitrary* (the choice of its final value assures the best numerical convergence).

The relation between these two surface parameters, A_{surf} and a_p, can be deduced from the equality, referring to figure A.1,

$$\frac{m_{L+\frac{d_0}{a_0}} - m_L}{d_0} = \frac{m_{L+1} - m_L}{a_0}; \tag{A.4}$$

or, after including (A.2) and (A.3),

$$\frac{m_L A_{surf} - m_L}{d_0} = \frac{m_L a_p - m_L}{a_0}. \tag{A.5}$$

After some rearrangements, the final formula is obtained from (A.5):

$$A_{surf} = (a_p - 1)\frac{d_0}{a_0} + 1. \tag{A.6}$$

In this study, the surface parameter A_{surf} values were calculated assuming d_0 in iron and nickel to be 1.435 and 1.76 Å, respectively (for plane (001)), according to [52].

References

[1] Joannopoulos J D, Meade R D and Winn J N 1995 *Photonic Crystals* (New York: Princeton University Press)
[2] Soukoulis C M (ed) 1996 *Photonic Band Gap Materials* (Dordrecht: Kluwer)
[3] Hillebrand R, Hergert W and Harms W 2000 *Phys. Status Solidi* b **217** 981
[4] McGurn A R 2000 *Phys. Rev.* B **61** 13235
[5] Kushwaha M S, Halevi P, Martinez G, Dobrzynski L and Djafari-Rouhani B 1994 *Phys. Rev.* B **49** 2313
[6] Vasseur J O, Djafari-Rouhani B, Dobrzynski L, Kushwaha M S and Halevi P 1994 *J. Phys.: Condens. Matter* **6** 8759
[7] Vasseur J O, Djafari-Rouhani B, Dobrzynski L and Deymier P A 1997 *J. Phys.: Condens. Matter* **9** 7327
[8] Tanaka Y and Tamura S 1998 *Phys. Rev.* B **58** 7958
[9] Tanaka Y and Tamura S 1999 *Phys. Rev.* B **60** 13294
[10] Vasseur J O, Dobrzynski L, Djafari-Rouhani B and Puszkarski H 1996 *Phys. Rev.* B **54** 1043
[11] Krawczyk M and Puszkarski H 1998 *Acta Phys. Pol.* A **93** 805
[12] Krawczyk M and Puszkarski H 1999 *Acta Phys. Superficierum* **3** 89
[13] Nikitov S A, Tailhades Ph and Tsai C S 2001 *J. Magn. Magn. Mater.* **236** 320
[14] Camley R E and Stamps R L 1993 *J. Phys.: Condens. Matter* **5** 3727
[15] Heinrich B and Bland J A C (eds) 1994 *Ultrathin Magnetic Structures II* (Berlin: Springer)
[16] Puszkarski H and Cottam M G 1991 *Acta Phys. Pol.* A **79** 549
[17] Vittoria C 1993 *Microwave Properties of Magnetic Films* (Singapore: World Scientific)
[18] Li B, Yang J, Shen J L and Yang G Z 1995 *J. Phys.: Condens. Matter* **7** 1405
[19] Hillebrands B, Harzer J V, Guntherodt C, England C D and Falco C M 1990 *Phys. Rev.* B **42** 6839
[20] Hillebrands B 1988 *Phys. Rev.* B **37** 9885
[21] Stamps R L and Camley R E 1996 *Phys. Rev.* B **54** 15200
[22] Anselmo D H, Cottam M G and Albuquerque E L 2000 *J. Phys.: Condens. Matter* **12** 1041
[23] Jouanne M, Szuszkiewicz W, Morhange J W, Kanehisa M A, Hartmann J M, Mariette H, Dynowska E, Karczewski G, Wojtowicz G, Kossut J and Barnas J 1998 *J. Cryst. Growth* **184/185** 947
[24] Heinrich B, Purcell S T, Dutcher J R, Urquhart K B, Cochran J R and Arrott S R 1998 *Phys. Rev.* B **38** 12879
[25] Litschke H, Schilberg M, Kleinefeld Th and Hillebrands B 1992 *J. Magn. Magn. Mater.* **104–107** 1807
[26] Schilberg M, Kleinefeld Th and Hillebrands B 1993 *J. Magn. Magn. Mater.* **121** 303
[27] Kordecki R, Meckenstock R, Pelzl J, Becker E, Dumpich G and Suran G 1991 *J. Magn. Magn. Mater.* **93** 281
[28] Krishnan R, Sella C, Kaabouchi M, Ramamurthy Acharya B, Prasad S and Venkatramani N 1992 *J. Magn. Magn. Mater.* **104–107** 1822
[29] Ramamurthy Acharya B, Prasad S, Venkatramani N, Kaabouchi M, Krishnan R and Sella C 1995 *J. Appl. Phys.* **78** 3992
[30] Zhai Y, Shi J, Zhang X Y, Shi L, Xu Y X, Huang H B, Lu Z H and Zhai H R 2002 *J. Phys.: Condens. Matter* **14** 7865
[31] Chambers A, Puszkarski H, Skinner A and Whiting J S S 1988 Spin-wave resonance in layered magnetic structures *12 ICMFS (Le Creusot)* paper ThP-37
[32] Draaisma H J G and de Jonge W J M 1988 *J. Appl. Phys.* **64** 3610

[33] Stancil D D 1993 *Theory of Magnetostatic Waves* (New York: Springer)
[34] Puszkarski H, Krawczyk M, Lévy J-C S and Mercier D 2001 *Acta Phys. Pol.* A **100** (*Suppl. 195*)
[35] Landau L D and Lifshitz E M 1975 *The Classical Theory of Fields* (Oxford: Pergamon) p 119
[36] Soohoo R F 1965 *Magnetic Thin Films* (New York: Harper and Row)
[37] Puszkarski H 1979 *Prog. Surf. Sci.* **9** 191
[38] Puszkarski H and Lévy J-C S 1990 *J. Phys.: Condens. Matter* **2** 4913
[39] Puszkarski H 1994 *Surf. Sci. Rep.* **20** 45
[40] Lévy J-C S 1981 *Surf. Sci. Rep.* **1** 39
[41] Damon R W and Eshbach J R 1961 *J. Phys. Chem. Solids* **19** 308
[42] Wolfram T and De Wames R E 1970 *Phys. Rev.* B **1** 4358
[43] Wolfram T and De Wames R E 1972 *Prog. Surf. Sci.* **2** 233
[44] Kalinikos B A and Slavin A N 1986 *J. Phys. C: Solid State Phys.* **19** 7013
[45] Kalinikos B A 1994 Dipole-exchange spin-waves spectrum of magnetic films *Linear and Nonlinear Spin Waves in Magnetic Films and Superlattices* ed M G Cottam (Singapore: World Scientific)
[46] Rado G T and Hicken R J 1988 *J. Appl. Phys.* **63** 3885
[47] Li S and Cross L E 1990 *Phys. Status Solidi* b **159** 861
[48] Hillebrands B 1990 *Phys. Rev.* B **41** 530
[49] Cochran J F, Heinrich B and Arrott A S 1986 *Phys. Rev.* B **34** 7788
[50] Gradmann U 1986 *J. Magn. Magn. Mater.* **54–57** 733
[51] Frait Z and Fraitová D 1988 Spin wave resonance in metals *Spin Waves and Magnetic Excitations Part 2* ed A S Borovik-Romanov and S K Sinha (Amsterdam: North-Holland) p 1
[52] Ashcroft N W and Mermin N D 1976 *Solid State Physics* (Holt: Rinehart and Winston)